EFFECTIVE CLEARANCE AND DIFFERENTIAL GAPPING IMPACT ON SEAL FLUTTER MODELLING AND VALIDATION

Roque Corral[†]
School of Aeronautics and Space
Universidad Politécnica de Madrid
28040 Madrid, Spain
e-mail: roque.corral@upm.es

Michele Greco[*]
School of Aeronautics and Space
Universidad Politécnica de Madrid
28040 Madrid, Spain
e-mail: michele.greco@upm.es

Almudena Vega[‡]
School of Aeronautics and Space
Universidad Politécnica de Madrid
28040 Madrid, Spain
e-mail: almudena.vega@upm.es

ABSTRACT

This paper presents an update of the model derived by Corral and Vega (2018, "Conceptual Flutter Analysis of Labyrinth Seal Using Analytical Models. Part I - Theoretical Support", *ASME J. of Turbomach.,* 140 (12), pp. 121006) for labyrinth seal flutter stability, providing a method of accounting for the effect of dissimilar gaps. The original CV model was intended as a conceptual model for understanding the effect of different geometric parameters on the seal stability comprehensively, providing qualitative trends for seal flutter stability. However, the quantitative evaluation of seal flutter, and the comparison of the CV model with detailed unsteady numerical simulations or experimental data, require including additional physics. The kinetic energy generated in the inlet gap is not dissipated entirely in the inter-fin cavity of straight-through labyrinth seals, and part is recovered in the downstream knife. This mechanism needs to be retained in the seal flutter model. It is concluded that when the theoretical gaps are identical, the impact of the recovery factor on the seal stability can be high. The sensitivity of the seal stability to large changes in the outlet to inlet gap ratio is high as well. It is concluded that fin variations due to rubbing or wearing inducing inlet gaps more open than the exit gaps lead to an additional loss of stability concerning the case of identical gaps. The agreement between the updated model and 3D linearized Navier-Stokes simulations is excellent when the model is informed with data coming from steady RANS simulations of the seal.

INTRODUCTION

Labyrinth seals are the most commonly used seal type in both gas and steam turbines due to their reliability to control leakage flows. They are made of non-contacting components consisting of a series of cavities connected by small clearances. The fluid is repeatedly forced to pass through these gaps generating kinetic energy that is dissipated in the down-stream inter-fin cavity. This process creates pressure losses that reduce the leakage flow through the seal.

Even though most of the studies regarding labyrinth seals are focused on sealing effectiveness (see [1] for a thorough review), it has been shown that seals are also a source of aeroelastic instabilities [2, 3, 4], though most of the seal failures are never disclosed by engine makers. Experimental analysis and post-mortem observations [5] show that seals are prone to flutter, and they represent a critical component of modern aero-engines. Ehrich [6] was one of the first authors to highlight the importance of fin clearance on seal stability. He proposed a simple analytical model neglecting the circumferential variations for a single seal cavity accounting for the effect of the geometry and the torsion center location concerning the seal center. Also, Lewis et al. [5] described the high sensitivity of seal stability to the knife-edge clearance, in particular to the most upstream one. Abbot [7] introduced the concept of acoustic circumferential resonances within the seal cavity giving rise to the well-known Abbot's criterion. However, he did not provide any theoretical model. One decade ago, di Mare *et al.* [8] introduced the systematic use of numerical simulations for the analysis of vibrating labyrinth seals.

Recently a new comprehensive physical-based seal flutter model

[†]Professor of Aerospace Engineering
[*]Corresponding Author
[‡]Also senior specialist at the Onshore Technology Development division of SIEMENS-Gamesa

has been proposed by Corral and Vega [9]. The CV model reconciliates the classical stability criteria of Ehrich and Abbot [7, 6] and provides more accurate and generic stability limits, including new dimensionless parameters. The model was further extended to stepped-seals [10] and applied to tip-shroud seals [11]. More recently, the formulation was updated, including the effect of non-isentropic unsteady perturbations and verified partially using CFD [12, 13]. Simultaneously, Miura and Sakai [14] have released a full set of experimental data obtained in a rotating rig.

All these seal flutter models and studies assume that the clearance of each fin is constant, but modern preliminary CFD studies [13] have shown that the effect of dissimilar gaps in seal stability can be of paramount relevance. Usually, labyrinth seals are designed to operate with equal nominal closures. However, due to the difficulties in controlling seal closures because of the disk and blade thermal excursions, in practice, the geometric closure of the different seal knives is never the same due to its tilting and leaning during operation. The demands for even higher efficiencies and performances in modern engines have led to more complex seal designs with very tight clearances, and therefore their relative displacements during operation with respect to the nominal gaps are currently higher than in the past.

Moreover, even under the assumption of geometrically equal gaps, the effective or fluid-dynamic gaps of the seal are never exactly the same because either the effective areas, i.e. the discharge coefficients, or the fraction of the wall-jet kinetic energy that is not dissipated in the inter-fin cavity and is carried-over to the downstream fin are different from knife to knife. This latter effect can also be translated into an equivalent effective area as well. In this context, a qualitatively correct leakage model for each fin is essential.

The original CV model already accounted for the effect of dissimilar gaps [15] but the implications on seal stability were never discussed.

This work firstly presents a method to estimate the effective flow passage area of the seal. The effective clearance of each gap is included in a new version of the CV flutter model. Then, the impact of dissimilar effective gaps on the seal stability is studied, comparing the prediction of the new formulation with the case of nominally identical gaps. The robustness of the seal to small perturbations of the gaps is discussed, and several conclusions are drawn. Finally, the updated model is compared to 3D linearized Navier-Stokes simulations.

LEAKAGE FLOW MODEL

The ideal mass flow, $\dot{m}_{id}$, through the i^{th} fin of the inter-fin cavity of the seal,assuming that the flow is isentropic and adiabatic, can be written as:

$$\dot{m}_{id,i} = \frac{P_{0,i} A_i}{\sqrt{R_g T_0}} \pi_i^{-\frac{\gamma+1}{2\gamma}} \sqrt{\frac{2\gamma}{\gamma-1}\left(\pi_i^{\frac{\gamma-1}{\gamma}} - 1\right)} \qquad (1)$$

where the subscript 0 refers to the total properties upstream of the fin and $\pi_i = P_{0,i}/p_i$ is the pressure ratio across the fin. The baseline CV model [9] makes the hypothesis that the kinetic energy of the incoming jet is fully dissipated in the cavity, the velocity in the inter-fin cavity is null, and then the total pressure of the cavity equals the static pressure. This hypothesis is used to compute the mass-flow through the downstream fin of the cavity. Nevertheless, in practice, for straight-through seal configurations, there is a significant amount of the wall-jet kinetic energy that is carried over to the downstream gap. This is especially true when the distance between two consecutive teeth is short and, the inter-fin cavity cannot mix out the jet. The so-called kinetic energy carry-over coefficient, χ, measures the cavity capacity to dissipate the jet kinetic energy. For stepped or staggered configurations, the wall-jet is not aligned with the downstream gap, therefore the assumption that the kinetic energy of the jet is fully dissipated is fulfilled frequently.

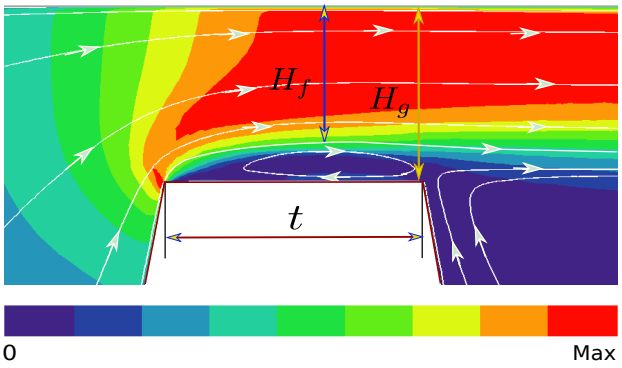

FIGURE 1. CONTRACTION OF THE STREAMLINES AT THE FIRST FIN TIP OF A LABYRINTH SEAL COLORED WITH THE MACH NUMBER ISO-CONTOURS.

Moreover, the throttling process through each seal fin leads to a contraction of the fluid, as it can be seen in Fig. 1. As a consequence, the effective passage area of the flow through the fin is smaller than the geometric seal area.

Kinetic energy carry-over coefficient

Hodkinson [16] proposed a model to account for the fraction of kinetic energy carried over from a seal inter-fin cavity to the next, χ. He assumed that the jet flow expanded conically into the cavity, departing from the upstream tooth, with a small angle, β (see Fig. 2 (a)). The rationale of the idea is that the longer the dimensionless distance from the upstream to the downstream knife,

H/L, the higher the dissipation of the wall-jet and, the lesser energy is recovered. The angle β is the spreading rate of the wall-jet what is directly related to the dissipated energy. Hodkinson [16] related the fraction of the dynamic head which is carried-over to the downstream tooth of a seal with identical gaps with the geometry and β as :

$$\chi = \frac{H}{H + L\tan\beta} \tag{2}$$

where H is the nominal seal clearance. In the case of a seal with dissimilar gaps, the proper choice of H in the expression 2 is the inlet gap of the cavity, $H = H_1$. The main idea is that the sensitivity of boundary layer type flows to downstream information is negligible because the problem is parabolic. Therefore, it is deemed that χ does not depend on the downstream gap, H_2. The effective total pressure of the cavity, P_{c0}, seen by the downstream fin is:

$$P_{c0} = p_c + \chi\,(P_0 - p_c). \tag{3}$$

If $\chi = 0$, the effective total pressure of the inter-fin cavity coincides with the static pressure of the cavity whereas if $\chi = 1$, the effective total pressure driving the jet flow through the downstream fin is P_0. Figure 2 (b) compares the carry-over coefficient obtained with a RANS analysis [17] using a fair resolution for the gap. The CFD results were post-processed in two different manners. First, χ was derived from the CFD using Eq. 3 where P_{c0} was obtained from the middle point of the downstream gap, which is outside of the boundary layer region (□ symbols in Fig. 2 (b)). This form of deriving χ from the CFD is more robust than determining the angle β of the dividing line between the wall-jet and the cavity recirculating flow and using Eq. 2 (◯ symbols in Fig. 2 (b)). In this case the angle $\beta = 0.033$ rad and is nearly constant for all the simulations. The agreement in the trend of χ with L/H_1 is reasonably good considering that no especial effort has been made to tune the results. The offset between the curves is not relevant since is finally removed from the model when the χ derived from the CFD is used. The dashed line in Fig. 2 (b) is obtained using Eq. 2 and selecting $\beta = \beta_{opt}$ to reproduce the χ obtained from proper post-processing of the CFD results (Eq. 3). The dependence of χ with the pressure ratio has been checked using CFD and is weak and in line with the works of other authors [18]. The trend of Eq. 2 is believed to be good enough for this work.

It will be seen, that Eq. 2 is only used to derive the functional dependence of P_{c0} with the geometry. The actual value of β is removed from the formulation at the end, and only the carry-over coefficient derived from the CFD is used.

Discharge coefficient

The discharge coefficient is defined as the ratio between the actual mass-flow, $\dot{m}$, and the mass-flow in ideal conditions, $\dot{m}_{id}$. It

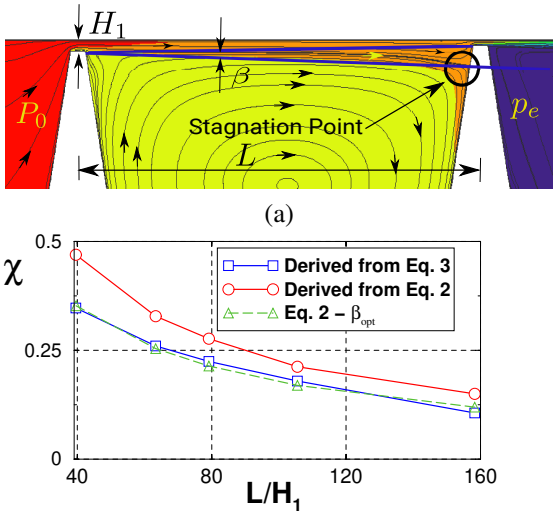

FIGURE 2. (A) SKETCH OF THE WALL JET EXPANSION ON THE INTER-FIN CAVITY WITH THE TOTAL PRESSURE FIELD SUPERIMPOSED WITH THE STREAMLINES FOR A SEAL WITH $H_{2,g}/H_{1,g} = 0.8$ OPERATING AT $\pi_T = 1.5$. (B) RECOVERY FACTOR , χ, DERIVED FROM 2D CFD ANALYSES AS A FUNCTION OF THE DIMENSIONESS CAVITY LENGTH. ◯: EQUATION 2 MODEL WITH $\beta = 0.033$ RAD DERIVED FROM Mu^2s^2T CODE [17]. □: χ, DERIVED FROM 2D RANS USING EQ. 3. △: EQ. 2 WITH $\beta_{opt} = 0.046$ RAD CHOSEN TO MATCH THE RESULTS OBTAINED WITH EQ. 3.

can be also interpreted as the ratio between the fluid-dynamic, A_f, and the geometric area, A_g, or in the case of a straight labyrinth seal, the ratio between the fluid-dynamic, H_f, and geometric gap, H_g (see Fig. 1),

$$C_d(Re_g, \text{Geometry}) = \frac{\dot{m}}{\dot{m}_{id}} = \frac{A_f}{A_g} = \frac{H_f}{H_g} \tag{4}$$

The discharge coefficient depends mainly but not only on the inlet geometry and the gap Reynolds number, Re_g.

The implicit assumption for the existence of the C_d is that the flow is uniform upstream. This is usually the case for the inlet fin since it ingests air coming from plenum-like conditions, but the situation is somewhat more complex for the outlet fin where a wall jet impinges directly in the exit gap. To evaluate the C_d, the actual mass flow rate, $\dot{m}$, is extracted from either experiments or numerical simulations while the ideal mass flow, $\dot{m}_{id}$, is calculated using Eq. 1 using an appropriate upstream total pressure.

The dependence of the leakage of a labyrinth seal upon the seal geometry and flow conditions was studied by Suryanarayanan and Morrison [18]. They provided a leakage correlation that was validated against prior experiments. The discharge coefficient resulted to be a function of the Reynolds number, the clearance to pitch ratio, and the clearance to fin thickness ratio,

$C_d = C_d(Re, H/L, H/t)$. Szymanski et al. [19] showed experimentally that the discharge coefficient of the seal depended as well on the pressure ratio.

Though not explicitly mentioned in [9], the gaps used in the CV model refer to the fluid dynamic gaps:

$$H_{1,f} = C_{d1} H_{1,g} \quad \text{and} \quad H_{2,f} = C_{d2} H_{2,g}. \tag{5}$$

Retaining the discharge coefficient is of primary importance on the evaluation of seal flutter. The relevance is not only associated with a small modification of the geometric gap but with the fact that if $C_{d1} \neq C_{d2}$ a seal with nominally equal clearances behaves in practice as a seal with different inlet and outlet gaps. It will be shown that the sensitivity of the seal stability to the gap ratio, $H_{2,f}/H_{1,f}$, can be high, hence its relevance.

Impact on the Steady-State Flow

The governing equations and the general expression for the cavity pressure in the steady-state were presented in [9], and therefore they will not be repeated here for the sake of brevity. Only those parts which are modified by the carry-over coefficient and the discharge coefficients are highlighted here.

The mass conservation equation of the seal neglecting circumferential variations, $d/dt(\rho_c V_c) = \dot{m}_1 - \dot{m}_2$, can be written as:

$$\frac{d}{dt}(\rho_c V_c) = \frac{P_0 A_1}{\sqrt{R_g T_0}} f(P_0/p_c, \gamma) - \frac{P_{c0} A_2}{\sqrt{R_g T_0}} f(P_{c0}/p_e, \gamma) \tag{6}$$

where Eq. 1 has been used, the total pressure in the cavitiy, P_{c0}, is given by Eq. 3, and the fluid dynamic areas are related to the nominal gaps by:

$$A_1 = C_{d1} 2\pi R H_{1,g} \quad \text{and} \quad A_2 = C_{d2} 2\pi R H_{2,g}. \tag{7}$$

The steady solution is obtained imposing that $\dot{m}_1 = \dot{m}_2$ in Eq. 6 from where an expression to estimate the inter-fin cavity pressure ratio at the steady-state, $\pi_s = P_0/p_c$, can be obtained:

$$\pi_s^{-\frac{\gamma+1}{\gamma}} \left(\pi_s^{\frac{\gamma-1}{\gamma}} - 1 \right) = \left(\frac{A_2}{A_1} \right)^2 \frac{1}{\pi_{s0}^2} \left(\frac{\pi_T}{\pi_{s0}} \right)^{-\frac{\gamma+1}{\gamma}} \left[\left(\frac{\pi_T}{\pi_{s0}} \right)^{\frac{\gamma-1}{\gamma}} - 1 \right] \tag{8}$$

where , $\pi_T = P_0/p_e$ is the seal pressure ratio, defined as the ratio between the inlet total pressure and the static pressure at the exit of the seal, and $\pi_{s0} = P_0/P_{c0}$ is the ratio between the upstream total pressure and the inter-fin cavity effective total pressure. Retaining the effective area of the gaps and the kinetic energy carried over modifies the steady pressure of the inter-fin cavity when compared with the baseline prediction of the original CV model.

The expression derived for the inter-fin cavity static pressure in Eq. 8 is valid as long as the seal is not choked, i.e. $P_{c0}/p_e \leq ((\gamma+1)/2)^{\gamma/(\gamma-1)}$. For higher values of the cavity pressure ratio, the flow through the last seal fin is choked and the exit mass flow is constant. Therefore, for the choked condition the following relationship is satisfied:

$$\pi_s^{-\frac{\gamma+1}{\gamma}} \left(\pi_s^{\frac{\gamma-1}{\gamma}} - 1 \right) = \left(\frac{\gamma-1}{2} \right) \left(\frac{A_2}{A_1} \right)^2 \frac{1}{\pi_{s0}^2} \left(\frac{\gamma+1}{2} \right)^{-\frac{\gamma+1}{\gamma-1}}. \tag{9}$$

When the seal is choked, the kinetic energy recovery factor, χ, causes that the critical pressure ratio of the seal, π_s^*, is not universal anymore, contrary to what is described in the original CV model formulation. Figure 3 describes the correction to the static pressure ratio in the inter-fin cavity as a function of the kinetic energy fraction carried over for a seal with the same fluid-dynamic passage area at the inlet and the outlet ($A_1 = A_2$). The critical total pressure ratio across the seal π_T^* decreases χ since part of the energy of the jet is recovered whereas the pressure ratio accross the inlet fin, π_s^*, increases.

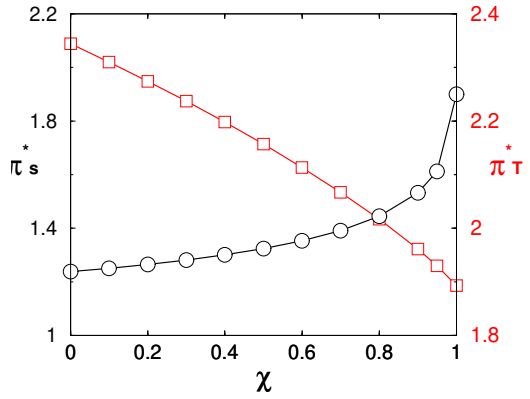

FIGURE 3. INTER-FIN SEAL CRITICAL STATIC PRESSURE RATIO $\pi_s^* = (P_0/p_c)^*$ (◯) AND CRITICAL TOTAL PRESSURE RATIO ACROSS THE SEAL, $\pi_T^* = P_o/p_e$, (□) AS A FUNCTION OF THE KINETIC ENERGY RECOVERY FACTOR , χ ($H_1 = H_2$).

It is important to recall that the steady-state description embedded in the CV mode is simple, and not critical for its use. The mean flow is taken usually from a steady CFD simulation or a more sophisticated air system model of the seal.

CARRY-OVER IMPACT ON THE LINEARIZED UNSTEADY MODEL

The original CV model linearizes the mass and momentum integral equations for a control volume, V_c, which represents a section of the inter-fin cavity of a rotating seal (see Figure 4) retaining the circumferential unsteady flow perturbations created by the seal vibration motion. The model assumes that the vibration amplitude of the seal is small enough, and therefore the flow and geometric variables can be decomposed into two parts: a steady

or mean background flow, plus a small and periodic unsteady perturbation. Therefore, the static pressure, the cavity volume, and the seal gap area can be written as follows:

$$p_c = p_{c,s} + p'_c(t),\ V_c = V_{c,s} + v_c(t),\ A_j = A_{j,s} + a_j(t). \quad (10)$$

Similarly, the kinetic energy recovery factor and the inter-fin cavity total pressure can be expressed as:

$$\chi = \chi_s + \chi'(t),\ P_{c0} = P_{c0,s} + P'_{c0}(t) \quad (11)$$

By using χ_s defined in Eq. 2, the perturbation of the kinetic energy recovery factor can be written as follows:

$$\chi' = (1-\chi_s)\hat{H}'_1 \quad (12)$$

where $\hat{H}'_1 = H'_1/(H_1 + L\tan\beta)$. Finally the perturbed effective pressure of the seal, P'_{c0}, is defined as:

$$P'_{c0} = \chi'(P_0 - p_c) + p'_c(1-\chi_s). \quad (13)$$

The implicit assumption of this formulation is that the residence time of the particles in the inter-fin cavity is small compared to the characteristic time of the vibration and therefore the process is deemed quasi-stationary. If the right hand side of Eq. 6 is linearized, the mass conservation equationcan be written as:

$$\frac{1}{\dot{m}_s}\frac{d}{dt}(\rho_c V_c) = -h(\pi_s)\frac{p'_c}{p_{c,s}} - J\left(\frac{\pi_T}{\pi_{s0}}\right)\frac{P'_{c0}}{P_{c0}} + \frac{a_1}{A_{1,s}} - \frac{a_2}{A_{2,s}} \quad (14)$$

where $h(\pi_s)$ and $J(\pi_T/\pi_{s0})$ are known expressions of the pressure ratio:

$$h = \frac{\gamma-1}{2\gamma}\left[\frac{\pi_s^{\frac{\gamma-1}{\gamma}}}{\pi_s^{\frac{\gamma-1}{\gamma}} - 1} - \frac{\gamma+1}{\gamma-1}\right] \quad (15)$$

$$J = \frac{\gamma-1}{2\gamma}\left[1 + \frac{(\pi_T/\pi_{s0})^{\frac{\gamma-1}{\gamma}}}{(\pi_T/\pi_{s0})^{\frac{\gamma-1}{\gamma}} - 1}\right] \quad (16)$$

(see appendix A of reference [9] for further details). Injecting Eqs. 12 and 13 into Eq. 14, it is readily obtained that:

$$\frac{1}{\dot{m}_s}\frac{d}{dt}(\rho_c V_c) = -h'\frac{p'_c}{p_{c,s}} - \psi\chi' + \frac{a_1}{A_{1,s}} - \frac{a_2}{A_{2,s}} \quad (17)$$

where h' and ψ are nondimensional functions defined as:

$$h' = h + J\frac{(1-\chi_s)}{\pi_s\chi_s + (1-\chi_s)},$$
$$\psi = J\frac{(\pi_s - 1)}{\pi_s\chi_s + (1-\chi_s)} \quad (18)$$

The variable h', that was defined in previous works [9] as $h' = 1+h$, has been generalized here to retain the effect of the carry-over coefficient, and the fact that the seal may not be choked necessarily. Finally, combining Eq. 12 and Eq. 17 the mass conservation equation becomes:

$$\frac{1}{\dot{m}_s}\frac{d}{dt}(\rho_c V_c) = -h'\frac{p'_c}{p_{c,s}} + \frac{a_1}{A^*_{1,s}} - \frac{a_2}{A^*_{2,s}} \quad (19)$$

Comparing Eq. 19 with the mass conservation equation derived on the original CV model, it is clear that including the effect of the kinetic energy carried over on the model leads to a new expression for the pressure ratio dependent funcion, h',and to a rescaling of the fluid-dynamic passage area as follows:

$$A^*_{1,s} = 2\pi R H^*_{1,s} = \frac{C_{d,1}A_{1,g}}{1-\psi(1-\chi_s)\chi_s}$$
$$A^*_{2,s} = 2\pi R H^*_{2,s} = C_{d,2}A_{2,g} \quad (20)$$

It can be seen that the new expression derived for the semi-linearized continuity equation (Eq. 19) is formally equivalent to that derived in the original CV formulation [9] if the new variables $A^*_{1,s}$ and $A^*_{2,s}$ are used.

From here on the formulation is identical to that described in [9]. Though all the ideas are compatible with a more complex and accurate higher-order model [13], it was decided to explain the implications of the carry-over coefficient and the differential gap on the baseline model to ease the discussion. Next, a short and quick rationale of the model derivation is included for the sake of completeness. Emphasis is put to highlight the presence of dissimilar gaps.

The nondimensional linearised mass conservation equation (Eq. 19) can be expressed as:

$$\Omega\left[\frac{\partial\tilde{p}}{\partial\tau} + \gamma\frac{\partial\tilde{v}_c}{\partial\tau} + \frac{1}{St}\frac{\partial\tilde{v}'_\theta}{\partial\tilde{z}}\right] = -h'\tilde{p} + \tilde{a}_1 - \tilde{a}_2 \quad (21)$$

if the mass flow variations in the circumferential direction are included (see [9]) and the following nondimensional variables are used:

$$\tilde{p} = \frac{p'_c}{p_{c,s}},\ \tilde{v}_c = \frac{v_c}{V_{c,s}},\ \tilde{a}_j = \frac{a_j}{A^*_{j,s}},\ \tilde{v}'_\theta = \frac{\gamma v'_\theta}{a_0},\ \tilde{z} = \frac{zND}{R},\ \tau = \omega t \quad (22)$$

where Ω is the non-dimensional discharge time of the cavity volume:

$$\Omega = \omega\frac{p_{c,s}V_{c,s}}{\dot{m}_s a_0^2} = \omega t_d. \quad (23)$$

The seal motion is deemed as a rotation about an arbitrary torsion center, aligned with the center of the seal and located at a certain distance r, from its center (see Fig. 4). The time variations of the inlet and outlet areas, $A_{1,2}(t,z)$, and the control volume, $V_{c,2D}(t,z)$, can be expressed in non-dimensional form as:

$$\tilde{a}_{1,2} = \frac{(r \pm L/2)}{H^*_{1,2}}\theta$$
$$\tilde{v}_c = \frac{r}{s}\theta \quad (24)$$

where L and s are the inter-fin cavity length and height, respectively.

The model considers the existence of different clearances for the inlet and outlet teeth, H^*_1 and H^*_2, respectively. To avoid overloading of the nomenclature, we will use from now on $H_j = H^*_j$ in

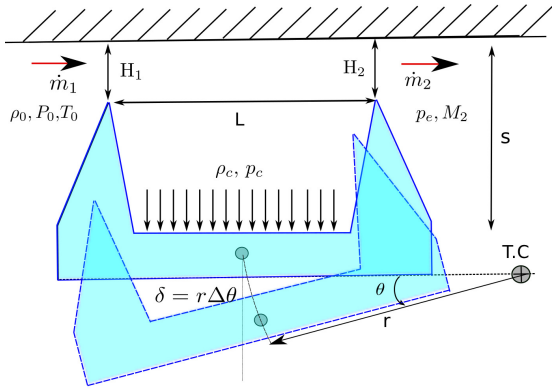

FIGURE 4. SKETCH OF AN IDEAL LABYRINTH SEAL SUPPORTED ON THE LPS

the understanding that the actual expressions are the ones given in Eq. 20. However, when the general formulation was introduced in [9], from the very beginning it was assumed that both clearances were identical to simplify the formulation, reduce the number of dimensionless parameters and ease the discussion of the new model. The effect of the existence of dissimilar gaps was reduced to a brief comment in the Eq. 12 of the second part of the paper [15].

If the motion of the seal is harmonic the torsion angle of the seal varies as $\theta = \Delta\theta \sin\tau$, and the forcing term on the right hand side of Eq. 21 can be expressed as follows:

$$\tilde{a}_1 - \tilde{a}_2 = \left[\frac{(r+L/2)}{H_1} - \frac{(r-L/2)}{H_2}\right]\Delta\theta\sin\tau = \frac{L}{H_{1,eff}}\Delta\theta\sin\tau \tag{25}$$

The effect of the dissimilar gap is included by introducing a new term, $H_{1,eff}$, defined as:

$$\frac{H_{1,eff}}{H_1} = \frac{2\eta}{2(\eta-1)r/L+(\eta+1)} \tag{26}$$

where

$$\eta = \frac{H_2}{H_1} \tag{27}$$

is the seal gap ratio. The dimensionless seal clearance or torsion center parameter introduced in [9] can be redefined as

$$\tilde{e}_{eff} = \gamma\frac{rH_{1,eff}}{sL} = \gamma\frac{rH_1}{sL}\left(\frac{H_{1,eff}}{H_1}\right) = \tilde{e}_1\left(\frac{H_{1,eff}}{H_1}\right) \tag{28}$$

and therefore:

$$\frac{\tilde{e}_{eff}}{\tilde{e}_1} = \frac{2\eta}{2(\eta-1)r/L+(\eta+1)} \tag{29}$$

The relevance of the above expression is that the sign of the effective dimensionless torsion center, $\tilde{e}_{eff}$, depends not only on the support side of the seal but also on the relative value of both clearances, which is a new conclusion of this paper. This represents a relevant change on the stability behavior compared to the prediction of the original CV model where this effect was not retained. Eq. 29 shows that if r/L is large but positive and $\eta < 1$, the effective distance to the torsion center can change sign. This effectively means that a seal supported physically in the LPS can behave in practice like a seal supported in the HPS. Keeping this in mind Eq. 21 becomes:

$$\tilde{\Omega}\left[\frac{d\hat{p}}{d\tau} + \tilde{e}_{eff}h'\cos(\tau+\tilde{z}) + \frac{1}{St}\frac{\partial\hat{v}'_\theta}{\partial\tilde{z}}\right] = -\hat{p} + \sin(\tau+\tilde{z}) \tag{30}$$

where the non-dimensional discharge time is scaled taking into account the effect of the pressure ratio, $\tilde{\Omega} = \Omega/h'^*$, and the unsteady pressure and the azimuthal velocity are renormalized as

$$\hat{p} = \frac{1}{\varepsilon}\tilde{p},\ \hat{v}'_\theta = \frac{1}{\varepsilon}\tilde{v}'_\theta \text{ with } \varepsilon = \frac{L\Delta\theta}{H_{1,eff}h'} \tag{31}$$

The linear approximation imposes that the unsteady pressure perturbations are small when compared with the seal mean pressure, $p_{c,s}$, and therefore the model requires that $\varepsilon \ll 1$.

Using the dimensionless variables introduced in Eq. 31,an expression of the dimensionless work-per-cycle similar to that described in [9] is derived:

$$\tilde{W}_{cyc} = \frac{W_{cyc}}{\pi p_{c,s}\delta^2 SL/\left|rH_{1,eff}\right|h'} = \text{sign}(rH_{1,eff})\hat{p}_c \tag{32}$$

where $\delta = r\Delta\theta$ is the seal torsion displacement, and $S = 2\pi RL$, is the surface of the seal land. All the parameters involved in the previous expression are sketched in Fig. 4. The dimensionless out-of-phase component of the unsteady pressure outlined in the original CV model is redefined by using the new expression for the nondimensional seal clearance, $\tilde{e}_{eff}$, and the fuction h' as:

$$\hat{p}_c = -\tilde{\Omega}\left[\tilde{e}h' + \left(1 - \frac{1}{St^2}\right)\right] \Big/ \left[1 + \tilde{\Omega}^2\left(1 - \frac{1}{St^2}\right)^2\right]. \tag{33}$$

The dimensionless work-per-cycle depends on three nondimensional parameters:

$$\tilde{W}_{cyc} = \tilde{W}_{cyc}\left(\tilde{\Omega}, St, \tilde{e}_{eff}h'\right) \tag{34}$$

but $\tilde{e}_{eff}h' = f(\tilde{e}_1 h', \eta, r/L)$. The impact of the effective clearance on the stability of the seal is derived by using the isentropic formulation described in [9] for the sake of simplicity. The modification to the original CV formulation discussed in this paper could be also applied on the non-isentropic version of the model described in [12].

The new definition of the seal non-dimensional effective clearance or torsion center accounts for the contribution of the differential gapping on the stability of the seal. The difference can be due to either the geometry or the fluid dynamic behaviour. The fluid dynamic difference between nominally identical inlet and outlet gaps has its origin in the inlet contraction due to the flow separation in the seal teeth (see Fig. 1) and in the partial dissipation of the kinetic energy in the inter-fin cavity which create an

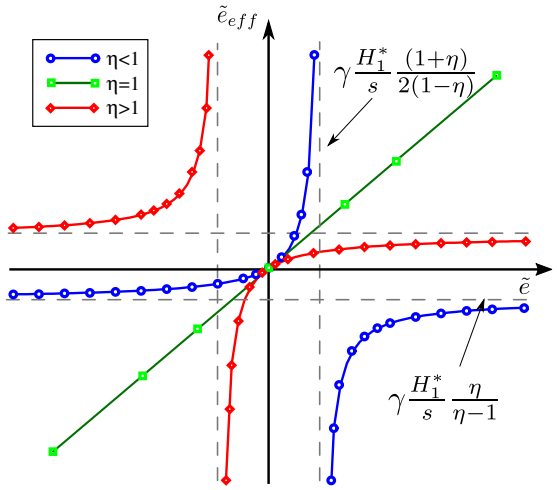

FIGURE 5. EFFECTIVE VERSUS ACTUAL NONDIMENSIONAL CLEARANCE OR TORSION CENTER DISTANCE FOR DIFFERENT INLET TO OUTLET GAP RATIOS, η.

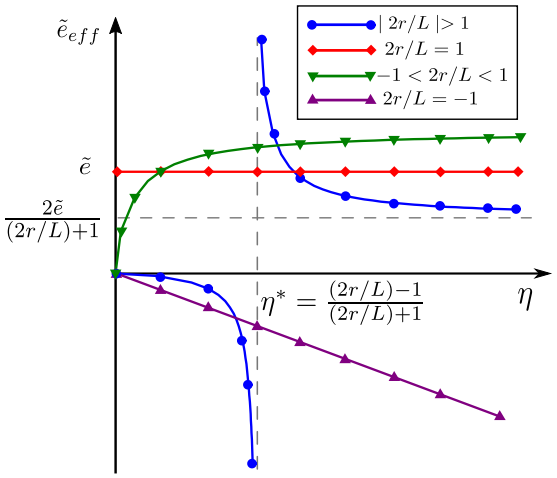

FIGURE 6. EFFECTIVE TO GEOMETRIC NONDIMENSIONAL SEAL CLEARANCE RATIO AS A FUNCTION OF THE GAP RATIO, η, FOR CHARACTERISTIC VALUES OF r/L.

asymmetry between the inlet and outlet gaps. Next section analyses the impact of the gap ratio on the effective non-dimensional clearance or torsion center $\tilde{e}_{eff}$.

IMPACT OF DIFFERENTIAL GAPPING ON THE EFFECTIVE TORSION CENTER

As it has already been mentioned, even if the geometrical gaps are identical, i.e. $H_{1,g} = H_{2,g}$, the fluid dynamic gaps, H_1 and H_2, can be different because either the discharge coefficients of the upstream and downstream gaps are different, $C_{d,1} \neq C_{d,2}$, or the carry-over coefficient is not zero (see Eq. 20).

The C_d variation between the inlet and outlet fins can be about 5-10%, while the carry-over coefficient can be up 20% or even larger, depending on the seal geometry. As a result, the variation of the geometric gap ratio, $\eta_g = H_{2,g}/H_{1,g}$, due to fluid dynamic effects can be up to 30% easily. In this work, it is considered that the analysis of the problem in the range of $0.5 < \eta < 2$ suffices since when the gap ratio is either very small or very large, the seal behaves as a single-fin seal which is a completely different problem.

The expression for $\tilde{e}_{eff}$ (Eq. 29) can be re-written in terms of $\tilde{e}_1$ assuming that $\bar{s} = s/(\gamma H_1 h')$ as

$$\tilde{e}_{eff} h' = \frac{2\eta \tilde{e} h'}{2(\eta-1)\bar{s}\tilde{e}h' + (\eta+1)}. \tag{35}$$

Figure 5 presents the correction to the nondimensional seal clearance of the original CV model due to seal dissimilar gaps, i.e $\tilde{e}_{eff}h'$ versus $\tilde{e}h'$ (see Eq. 35) for a constant seal geometry so that $\bar{s}$ is constant, and the change of $\tilde{e}h'$ shall be understood as a change of the torsion center. The most striking outcome is that the corrected effective nondimensional clearance, $\tilde{e}_{eff}$, can change its sign with respect to the original parameter of the CV model, $\tilde{e}$, depending on the seal supporting side and the outlet to inlet clearance ratio, η. For $\eta = 1$, $\tilde{e}_{eff} = \tilde{e}$ and a straight line is obtained. However, if $\eta < 1$ (blue line with circle symbols), the seal is supported in the LPS and the torsion center is located sufficiently far away (recall that $\tilde{e} = \gamma Hr/(sL)$), $\tilde{e}_{eff}$ becomes negative if

$$\tilde{e} > \gamma \frac{H_1^*}{s} \frac{(1+\eta)}{2(1-\eta)}. \tag{36}$$

This actually means that a seal supported on the LPS can behave in terms of stability as a seal supported on the HPS which can make simulation and experimental data difficult to interpret. The difficulty does not lie neither in the simulation system nor in the model itself since both can handle smoothly dissimilar gaps. The problem is interpreting the results and their relationship with the case of equal gaps, where an engineering intuition based on the model has been created yet.

Figure 6 displays the effective nondimensional seal clearance parameter, $\tilde{e}_{eff}$, as a function of the gap ratio, η, for four different characteristic scenarios defined by the position of the torsion center (Eq. 29).

The first observation is, that the sign of $\tilde{e}_{eff}$ is only affected by the gap ratio when the physical torsion center is located outside the inter-fin cavity, i.e. $|r/L| > 0.5$. In this case, $\tilde{e}_{eff}$ has a singularity when $\eta^* = \frac{2r/L-1}{2r/L+1}$, and a change in its sign. Another way of looking at the problem is for given gap ratio, the dimensionless radius of the torsion centre, $(r/L)^*$, at which the effective

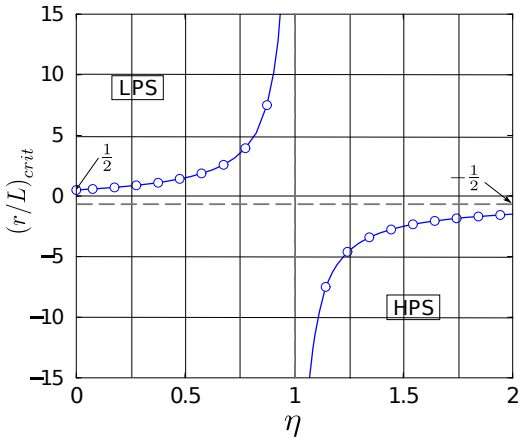

FIGURE 7. CRITICAL VALUE OF THE TORSION CENTER POSITION AS A FUNCTION OF THE SEAL GAP RATIO, η.

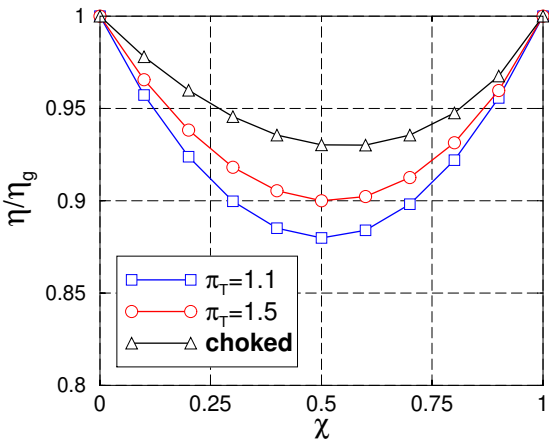

FIGURE 8. IMPACT OF THE KINETIC CARRY-OVER COEFFICIENT ON THE MODEL GAP RATIO

torsion center or radius, $\tilde{e}_{eff}$, changes sign is:

$$\left(\frac{r}{L}\right)_{crit} = \frac{1}{2}\frac{1+\eta}{1-\eta}. \tag{37}$$

This effectively means that if for whatever reason the effective gap ratio changes by 15%, such for instance a C_d variation, at $|r/L|^* \gtrsim 7$ the behaviour of the seal is opposite as expected. Figure 7 displays this critical radius as a funcion of η. The asymptotic value of $\tilde{e}_{eff}$ when $\eta \to \infty$ is

$$\lim_{\eta\to\infty} \tilde{e}_{eff} \to \frac{2\tilde{e}}{2r/L+1} \tag{38}$$

which is the same for all the cases. Nevertheless, it must be noted that large values of η are not very realistic in seal design, as it has been previously commented.

Another interesting observation is that when the torsion center is located at the exit of the seal cavity, $r/L = 0.5$, the effective dimensionless torsion center is independent of the gap ratio, i.e. $\tilde{e}_{eff} = \tilde{e}$, and the sensitivity of the seal to dissimilar gaps is small.

On the other hand, if the torsion center is located at the inlet of the seal cavity, $r/L = -0.5$, the effective dimensionless torsion center is $\tilde{e}_{eff} = -\frac{\gamma H_1}{2s}\eta$ and the effective torsion center is always negative, independently of η.

Finally, it must be said that an accurate quantification of the effective clearances is of major relevance since a wrong estimation of the outlet to inlet gap ratio can lead to misleading conclusions regarding seal stability.

Carry-over Coefficient Impact on Gap Ratio

The effect of the carry-over coefficient on the model gap ratio is evaluated next. The seal fins are assumed to have the same geometric closure, $H_{1,g} = H_{2,g}$, and the same discharge coefficients, $C_{d1} = C_{d2}$ and therefore, the fluid dynamic gaps are the same. However, the kinetic energy recovered in the downstream gap has an impact on the gaps of the model which is retained by using expressions 18 and 20. Even in this simplified case, the ratio between the effective gap ratio, η, and the geometric gap ratio, η_g,is a function of the kinetic carry-over coefficient and the pressure ratio, $\eta/\eta_g = \eta(\chi, \pi_T)$.

Figure 8 shows that the impact of χ on the gap ratio is always a slight reduction that peaks around $\chi = 0.5$. Typical values of χ oscillate between 10% and 20% and reductions in the gap ratio of 5-10% are easily seen. The impact is larger at low-pressure ratios what is somehow surprising. Though this impact seems to be small, it will be shown that these small variations can induce significant changes in seal stability. It is worth mentioning that the choked curve corresponds to different pressure ratios since the choking condition depends on the recovery factor.

STABILITY LIMIT CORRECTION

The stability analysis of the seal could be simply conducted estimating first the effective gap or torsion center, $\tilde{e}_{eff}$ as a function of the gap ratio, η, the dimensionless position of the torsion center, r/L, and the original torsion center parameter of any of the versions of the CV model [9, 10, 13] using the effective gaps formulated in Eq. 20. In the second place, use the the new definition of h' (see Eq. 18) taking into account the seal pressure ratio and the carry-over coefficient. Finally, use the expression of the work-per-cycle of the models or their stability criteria with all the information in place.

However, following this process little can be learned about the dependence of the seal stability trends with the design parame-

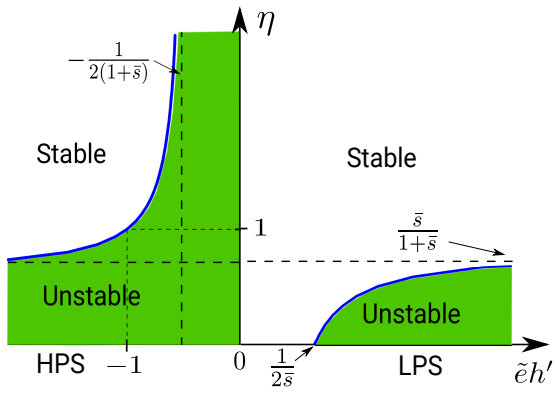

FIGURE 9. GAP RATIO EFFECT ON THE STABILITY CRITERION OF THE 0^{th} NODAL DIAMETER.

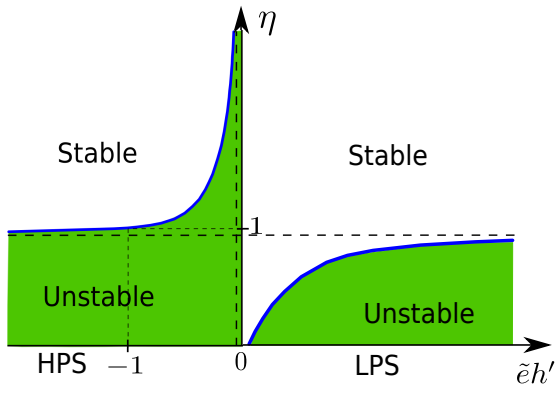

FIGURE 10. STABILITY CRITERION OF THE 0^{th} NODAL DIAMETER FOR HIGH VALUES OF THE NONDIMENSIONAL HEIGHT, $\bar{s} \gg 1$.

ters. It can be anticipated that when the effective inlet and outlet gaps of the model are different for whatever reason, the understanding of the stability trends with the dimensionless parameters is much more complex because not only a new parameter, η, appears but the original parameter $\tilde{e} = \gamma r H/(sL)$ is split into two, r/L and $\gamma H/s$. This means that in practice the stability depends on two more dimensionless parameters and some of them are functions of the C_d and χ coefficients. Therefore, although the model is analytic and based on algebraic expressions, this simplicity does not translate directly in a clear understanding of the problem. In this section, we will convey just a summary of the most relevant conclusions.

Zero nodal diameter stability criterion

The case of the zero nodal diameter is discussed first because of its simplicity, even if it represents a pathological case with little practical relevance. This limit can be obtained either neglecting the pressure perturbations on the circumferential direction or making the limit $St \to \infty$ in the baseline model [9]. The dimensionless work-per-cycle for this particular case can be written as:

$$\tilde{W}_{cyc} = \text{sign}(\tilde{e}_{eff}h')\hat{p}_c = -\text{sign}(\tilde{e}_{eff}h')(1+\tilde{e}_{eff}h')\frac{\tilde{\Omega}}{(\tilde{\Omega}^2+1)} \tag{39}$$

where the out-of-phase component of the pressure, $\hat{p}_c$, is derived from Eq. 33 in the limit $St \to \infty$. This expression is very similar to the one derived in [9], with the main difference that now the seal stability depends on two additional parameters, $\tilde{e}_{eff}h' = f(\tilde{e}h', \eta, \bar{s})$ (see Eq. 29). This new dependence directly implies that the $\tilde{W}_{cyc}$ can change its sign depending on the gap ratio, as it can be seen in Fig. 9, which shows the stability map for the 0^{th} nodal diameter as a function of the gap ratio, η.

According to the CV model, when $\eta = 1$, the 0^{th} ND of the seal is unstable only if $-1 < \tilde{e}h' < 0$. The new formulation reflects that if the clearances are different ($\eta \neq 1$) there are two key parameters that control the seal stability namely the dimensionless gap, $\bar{s} = s/(\gamma H h')$, and the gap ratio, η. It has been decided to retain the original parameter $\tilde{e}h'$ of the CV model among the three controlling parameters for the sake of continuity with previous work, although it must be emphasized that this single parameter does not collapse all the dependences anymore.

The new stability criterion can be formally expressed as:

$$\text{if } \tilde{e}h' \gtrless 0 \;\; \text{then } \eta \gtrless \frac{2\tilde{e}h'\bar{s}-1}{2\tilde{e}h'(1+\bar{s})+1} \tag{40}$$

Figure 9 displays the stable and unstable regions of the seal as a function of $\tilde{e}h'$, that can be interpreted as a sort of dimensionless torsion center, and the gap ratio. Note that the stability limit depends as well on $\bar{s}$. The first observation is that if the two gaps are identical ($\eta = 1$) the stability criterion of the classical CV model [9] is recovered. The LPS is always stable whereas the HPS is stable if $\tilde{e}h' < -1$. Secondly, it can be noticed that if the exit gap is larger than the inlet one ($\eta > 1$) the seal is more stable in the HPS but even for $H_2 \gg H_1$ there is always a residual unstable region in the HPS. However, if the exit gap is smaller than the inlet one ($\eta < 1$) the seal is less stable, and the LPS can become unstable. This trend is general and can be observed for other nodal diameters as well. The kinetic energy carried-over to the downstream fin entails that $\eta < \eta_g$, and hence a reduction of the stability margin.

It is important to notice that the dimensionless height, $\bar{s}$, is always high for most of the seals since s/H_1 is large necessarily. The general stability criterion for arbitrary values of $\bar{s}$ depicted in Fig. 9 can then be simplified. Figure 10 shows the stability criterion for the 0th *ND* when $\bar{s} \gg 1$. It can be seen, that the stability condition reduces in this case to $\eta \gtrsim 1$ approximately. The range in which the problem is stable if for some reason the outlet gap is slightly smaller than the inlet one is very small. In other words, the 0th *ND* tends to be always unstable in practice, independently

of the torsion center, though this instability tends to be weak.

General Stability Criterion

The critical reduced frequency is obtained by imposing that $\tilde{W}_{cyc}(St_c) = 0$, leading to the following expression:

$$St_c^2 = \frac{1}{1+\tilde{e}_{eff}h'} \tag{41}$$

which is a generalization of the criterion derived in [9] including the impact of the dissimilar gaps. Exactly as in the zero ND case the stability criterion can be expressed in terms of the classical $\tilde{e}h'$ parameter and the newly created parameters η and $\bar{s}$.

Figure 11 displays the stability regions as a function of the gap ratio η for clarity. Three cases are presented, two for $\eta < 1$ and one for $\eta > 1$.

Figure 11 (b) sketches the stability criterion in the range $(\bar{s}-1)/\bar{s} < \eta < 1$ which contains the baseline case with equal gaps. The curves in this case are alike those found in the baseline case ($\eta = 1$). The effect of decreasing the exit gap slightly, and therefore η, is to create a region on the LPS ($\tilde{e}h' > (\eta+1)/2s(1-\eta)$) which is stable irrespectively of the vibration-to acoustic frequency ratio, St. However, in the HPS, the region of unstable torsion centers is enlarged. The asymptote that separates the stable from the unstable regions on the HPS, and that is located at $\tilde{e}h' = \frac{1}{2}(\eta+1)/(\bar{s}(\eta-1)+1)$, moves to the left. As it has been already mentioned, often $\bar{s} \gg 1$ and the range of validity of this solution is a small region around $\eta \simeq 1$, i.e. $((1-\bar{s}^{-1}) < \eta < 1)$. This type of situation can be observed in straight seals with nominally identical gaps.

Figure 11 (a) represents a situation in which the exit gap has been intentionally reduced, or the inlet knife has been damaged and shortened, and $\eta < (\bar{s}-1)/\bar{s}$. In this situation, the asymptote moves to the LPS and the HPS will be always unstable since in practice the high NDs associated with high frequencies will become unstable. However, the low-frequency region is stable. On the LPS, if the frequency is low enough, there is an unstable region close to the origin, which becomes small for $\bar{s} \gg 1$, exactly as in the case of equal gaps. Nevertheless for torsion centers located slightly far away from the inter-fin cavity center the seal becomes unstable again for high frequencies. This instability cannot be avoided increasing the frequency of the seal but its mode-shape. This situation in which the inlet gap is increased in an uncontrolled manner, due to rubbing or contacts for instance, leads the seal towards a more unstable condition and is to be avoided.

The case in which the outlet gap, H_2, is larger than the inlet gap, is more benign since a stable region on the LPS for high enough frequencies of the seal always exists (see Fig. 11 (c)). Furthermore when the support is located on HPS, the unstable region

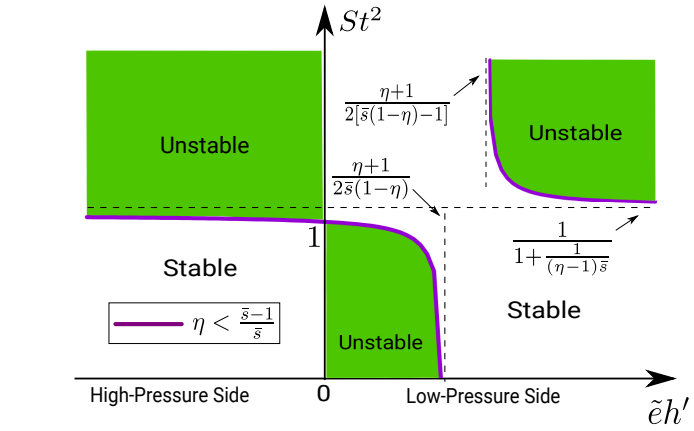

(a) $0 < \eta < (\bar{s}-1)/\bar{s}$

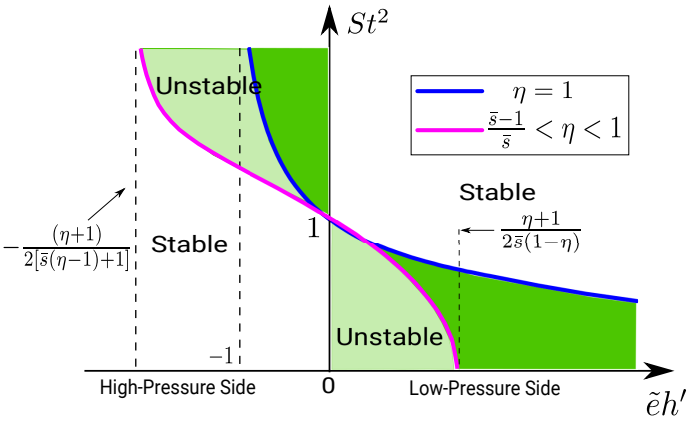

(b) $(\bar{s}-1)/\bar{s} < \eta < 1$

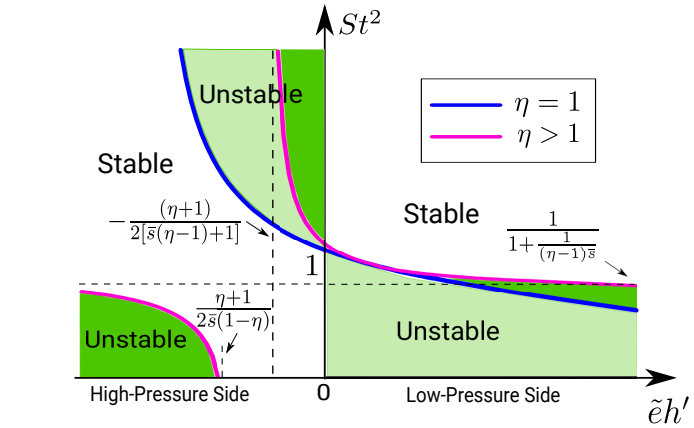

(c) $\eta > 1$

FIGURE 11. CV STABILITY CRITERION AS A FUNCTION OF THE DIMENSIONLESS TORSION CENTER ($\tilde{e}h'$) FOR DIFFERENT VALUES OF THE GAP RATIO

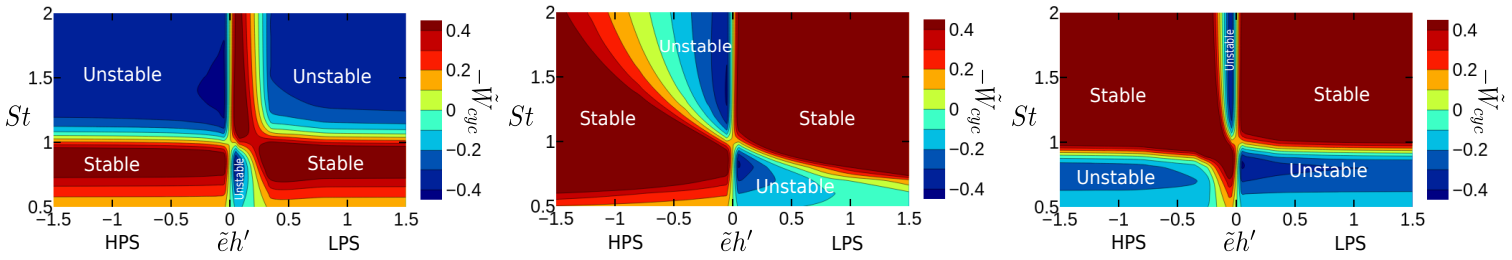

(a) $\eta = 0.5$ (b) $\eta = 1$ (c) $\eta = 2$

FIGURE 12. DIMENSIONLESS WORK-PER-CYCLE, $\tilde{W}_{cyc}$, FOR DIFFERENT GAP RATIOS AND LARGE DIMENSIONLESS SEAL HEIGHTS, $\bar{s} = 10$. THE NON-DIMENSIONAL DISCHARGE TIME IS $\tilde{\Omega} = 2.5$

outlined by the classical stability criterion is smaller. Conversely, for low frequencies and torsion centers relatively far away from the seal, a new unstable region is observed. This situation is more robust from a design point of view.

Figure 12 displays the maps of the dimensionless work-per-cycle for large values of the dimensionless seal height ($\bar{s} = 10$). Three types of seals corresponding to the cases $\eta = 0.5$, $\eta = 1$ and $\eta = 2$ are displayed in the Figs. 12 (a), (b) and (c) respectively. The same ideas sketched in Fig. 11 are actually computed here with the model. It can be observed that when the outlet gap is smaller than the inlet one (Fig. 12 (a)) the seal is always unstable for high frequencies, except in a small region in the LPS close to the origin. However, if the outlet gap is bigger than the inlet one (Fig. 12 (c)) the seal is stable for vibration-to-acoustic frequency ratios larger than one, except in a small region in the HPS in the vecinity of the origin.

The comparison of these maps with CFD simulations is presented in the next section. The reader can find some preliminary results in [12, 13] where it is shown that the level of agreeement between the model and three-dimensional linearized Navier-Stokes simulations [20] is very high.

NUMERICAL VERIFICATION

A thorough numerical verification of the model has been performed incrementally and systematically but its detailed presentation is outside of the scope of the paper. However, the simulations concerning just the impact of the dissimilar gaps in the stability, which are the more relevant for this work, are presented next. It important to warn the reader that the methodology presented here is critical for a wide range of configurations and operating conditions, except for stepped seals where $\chi \simeq 0$. All the analyses have been performed using a well-validated frequency-domain linearized Navier-Stokes solver [20]. The reader can find some preliminary results of the validation of the model in [12, 13] where it is shown that the level of agreement between the model and the simulations is very high.

Numerical Model

The semi-discretised RANS equations in compact form can be written as:

$$\frac{d(\mathbf{V}(t).\mathbf{U})}{dt} = \mathbf{R}(\mathbf{U}, \mathbf{A}(t), \mathbf{W}_c(t)) \tag{42}$$

where $\mathbf{V}$, $\mathbf{A}$ and $\mathbf{W}_c$ are vectors containing respectively the volumes, areas and face velocities of the cells, and $\mathbf{R}$ is the residual. Flow unsteadiness is caused by a small periodic motion of the solid walls, in this case of the seal. Since the mesh is conformal at any instant with the vibrating boundaries, a periodic deformation of the whole mesh is created. The grid dependent geometric factors can be decomposed into a steady or mean value plus a periodic perturbation, i.e.

$$\begin{aligned} \mathbf{V}(\mathbf{x},t) &= \mathbf{V}_0(\mathbf{x}) \ + \ \mathbf{v}(\mathbf{x},t) \\ \mathbf{A}(\mathbf{x},t) &= \mathbf{A}_0(\mathbf{x}) \ + \ \mathbf{a}(\mathbf{x},t) \\ \mathbf{W}(\mathbf{x},t) &= \mathbf{W}_0(\mathbf{x}) + \mathbf{w}(\mathbf{x},t) \end{aligned} \tag{43}$$

Since the vibration of the solid walls is deemed to be small $\mathbf{v}(\mathbf{x},t) \ll \mathbf{V}_0(\mathbf{x})$ and $\mathbf{a}_0(\mathbf{x}) \ll \mathbf{A}(\mathbf{x},t)$, and the mean velocity of the mesh is null, $\mathbf{W}_0(\mathbf{x}) = 0$. The solution, $\mathbf{U}(\mathbf{x},t)$, is decomposed as well into a mean base flow, $\mathbf{U}_0(\mathbf{x})$ and a small perturbation $\mathbf{u}(\mathbf{x},t) \ll \mathbf{U}_0$, which in turn can be expressed as a Fourier series in time. If just the first harmonic of the variations is retained, any variable can be expressed as

$$\mathbf{U}(\mathbf{x},t) = \mathbf{U}_0(\mathbf{x}) + \mathrm{Re}(\hat{\mathbf{u}}(\mathbf{x})e^{i\omega t}) \tag{44}$$

where $\hat{\mathbf{u}}$ is the complex perturbation, and ω is the angular frequency. The baseline solution is obtained solving the nonlinear problem $\mathbf{R}(\mathbf{U}_0, \mathbf{A}_0) = 0$ whereas the linear harmonic solution is obtained linearising Eq. 42 about $\mathbf{U}_0$ to obtain the complex linear problem:

$$i\omega \mathbf{V}_0 \hat{\mathbf{u}} + \left(\frac{\partial \mathbf{R}}{\partial \mathbf{U}}\right)_0 \hat{\mathbf{u}} = \hat{\mathbf{f}}(\mathbf{U}_0, i\omega) \tag{45}$$

where $\hat{\mathbf{f}}$ is a forcing term associated with the mesh deformation, and $(\partial \mathbf{R}/\partial \mathbf{U})_0$ is the Jacobian of the residual evaluated with the mean solution $\mathbf{U}_0$ obtained from the nonlinear solver. The details of the solver and validation results for other type of configurations can be found in [20, 21, 22]. The model and the unsteady

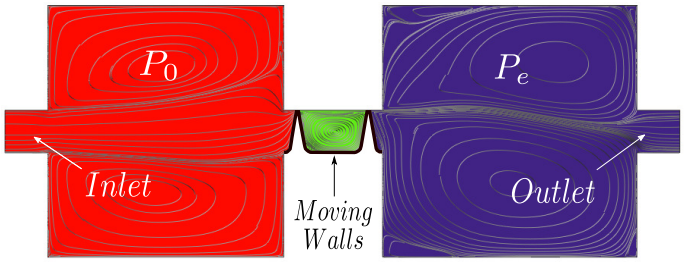

FIGURE 13. SKETCH OF THE COMPUTATIONAL DOMAIN WITH THE STEADY-STATE STREAMLINES FOR A SEAL OPERATING AT $\pi_T = 2.0$ COLOURED BY THE STATIC PRESSURE.

solver are both linear and therefore, the solutions are fully compatible since in both cases nonlinear unsteady interactions are neglected.

The frequency-domain linearised Navier-Stokes solver is spatially discretised using a MUSCL-like second-order finite volume method consistent with the matrix-valued form of the artificial viscosity. The eddy-viscosity is frozen in the linear solver and computed using the standar Wilcox 2006 $k-\omega$ model in the non-linear counterpart of the method [17].

Numerical Setting

A simplified geometry consisting in a two-fin straight-through non-rotating labyrinth seal has been used to verify the model. The computational domain includes upstream and downstream cavities that act as plenum chambers ensuring a uniform inlet and outlet pressure across the seal (see Fig. 13). The baseline seal geometry with identical geometric gaps is defined by $s/R = 0.018$, $s/H_g = 50$, $L/s = 5/3$, and $t = 3H_g$. Some more details can be found in [13].

Mesh Description The meridional plane displayed in Fig. 13 is discretized using an hybrid grid with 35,000 points. The model is extruded in the circumferential direction to form a 10° sector containing 10 layers. Therefore, the full mesh consists of 350,000 points. The standard $k-\omega$ turbulence model is integrated to the wall and the mesh is fine enough in the whole domain to ensure that $y^+ \simeq 1$. The seal geometry and the mesh are axisymmetric.

Mode-Shape Definition The CV model assumes that the seal mode-shape is a rigid body motion around a pivot point in the meridional plane. To ease the the simulation set up a synthetic mode-shape generator has been implemented. Once the axial torsion center distance and the ND are selected (The radial distance is irrelevant in a straight seal since it gives rise to an axial component motion of the seal [10]), the mode displacements are applied to the seal wall nodes and then transferred to the inner nodes using a Laplacian smother. This technique allows a full control of the mode-shape for conceptual studies. Phase-shifted boundary conditions are used in the azimuthal boundaries of the mesh to simulate arbitrary NDs in the 10° sector.

η_g	χ_s	C_{d1}	$C_{d,2}$	η	Re	$\bar{s}$	h'	Ω
1	0.23	0.97	0.93	0.84	21.000	10.7	3.32	11.1
4/3	0.18	0.98	0.92	1.05	18.800	13.8	3.34	12.3
2	0.1	1	0.92	1.48	13.000	11.6	6.13	15.8

TABLE 1. STEADY STATE DATA DERIVED FROM CFD NON-LINEAR ANALYSIS FOR DIFFERENT GAP RATIOS. THE PRESSURE RATIO IS KEPT CONSTANT, $\pi_T = 1.5$.

Results

The effect of the gap difference on the stability is explored numerically by varying the thickness of the first gap, keeping constant the downstream gap. The pressure ratio for three cases ($\eta_g = 1$, 4/3 and 2) has been set to $\pi_T = 1.5$. The vibration-to-acoustic frequency ratio, St, variation has been obtained by changing the ND keeping the frequency constant to avoid the contamination due to resonances of upstream and downstream cavities. The dimensionless torsion center, $\bar{e}h'$, has been varied by changing the torsion center distance, r.

Steady State Data The steady nonlinear simulations are used to feed the frequency-domain Navier-Stokes linearized analyses and to derive the discharge coefficients of each fin, the carry-over coefficient and other basic data needed to feed the model and non-dimensionalize the W_{cyc}, such as the mean pressure of the inter-fin cavity.

Table 1 shows the main steady data derived from the nonlinear analysis for three different geometric gap ratios, namely η_g =1, 4/3 and 2. The first observation is that the carry-over coefficient decreases when η_g is increased. This is due to the fact that H_1/L increases since H_2 is kept constant (see Eq. 2 and Fig. 2 (b)). The second observation is that the discharge coefficients are very high ($C_d \lesssim 1$) in this case. This is partially due to the fact the tip of fin is relatively thick leading to a high C_d (see [19]). In this case the ratio $C_{d,1}/C_{d,2} \sim 5-8\%$ and its role is small compared to that of the carry-over coefficient. In any case, the steady data obtained by the CFD are injected in the unsteady model and therefore most of the uncertainties associated with the steady validation of the code are removed from the comparison between the

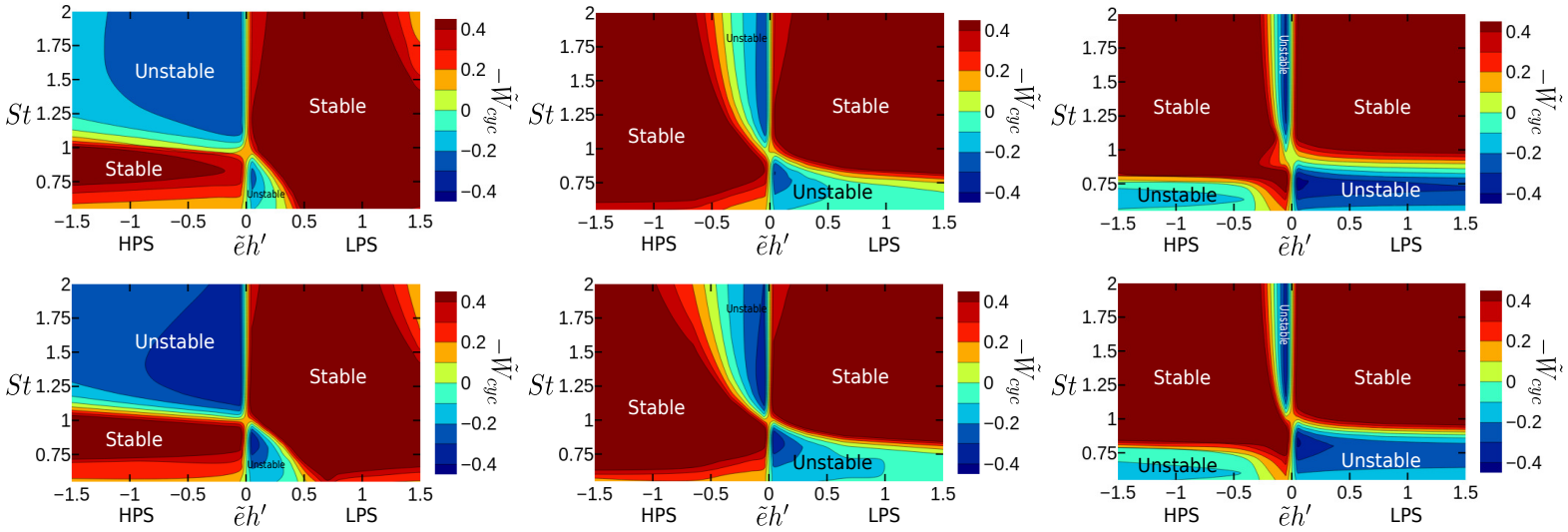

(a) $\eta_g = 1$ (b) $\eta_g = 4/3$ (c) $\eta_g = 2$

FIGURE 14. STABILITY MAPS ($\tilde{W}_{cyc}$) FOR A TWO-FIN STRAIGHT SEAL AS A FUNCTION OF THE DIMENSIONLESS TORSION CENTER, $\tilde{e}h'$, AND THE VIBRATION-TO-ACOUSTIC FREQUENCY RATIO, St, FOR DIFFERENT GEOMETRIC RATIOS OF THE GAPS (PRESSURE RATIO: $\pi_T = 1.5$). BOTTOM: CV HIGH-ORDER MODEL [12]. TOP: LINEARIZED NAVIER-STOKES RESULTS USING A SIMULATION MATRIX OF 15×17 CASES.

work-per-cycle obtained by the linearized Navier-Stokes solver and the model.

It is important to recall that the effective gap ratio to include in the model is $\eta = A^*_{2,s}/A^*_{1,s}$ which according to Eq. 20 turns out to be:

$$\frac{\eta}{\eta_g} = (1-\psi(1-\chi_s)\chi_s)\left(\frac{C_{d,2}}{C_{d,1}}\right) \tag{46}$$

The effective gap ratio is smaller than the geometric gap ratio due to the energy carried-over to the downstream fin (see Table 1). In fact the seal with nominally identical gaps behaves qualitatively as a seal with $\eta < 1$, whereas the seal with $\eta_g = 4/3$ behaves approximately as a seal with identical gaps ($\eta \simeq 1$) (See Fig. 14). This is the reason why is so important to retain the impact of the carry-over coefficient in the formulation.

Dimensionless Work-per-Cycle The CV model predicts the work-per-cycle performed by the inner walls that define the inter-fin cavity. However, the motion injected to the 3D unsteady simulations by the artificial generator of mode-shapes includes displacements of the outer fin walls (see Fig. 13). The work associated with the motion these external walls is disregarded in the CFD analysis to make a fair comparison with the model.

Figure 14 compares the dimensionless work-per-cycle obtained with the frequency-domain linearized Navier-Stokes solver [20] (top) with the higher-order model described in [12], updated with the carry-over corrections described in this work (bottom). A simulation matrix of 15 torsion centers and 17 NDs is used to construct each of the plots of the top row, totalling 765 simulations.

The work-per-cycle contours have been bounded in the range $-0.5 < -\tilde{W}_{cyc} < 0.5$, to enhance the visualization. Figure 14 shows that the matching of the CFD results with the prediction of the model is excellent for the three cases. The impact of the carry-over coefficient is clearly seen in the case of nominally identical gaps, $\eta_g = 1$. The recovery of kinetic energy in the exit fin makes that the effective gap ratio become $\eta = 0.84$. The stability pattern outlined in [9] for a seal with identical gaps changes completely and three different scenarios can be distinguished.

The first scenario is the seal with nominally identical geometrical gaps, $\eta_g = 1$, which is largely the most recurring case. The discharge coefficients of both fins are similar and their ratio close to the unity. The analytical model and the simulations predict that even if the discharge coefficients of both gaps are nearly identical, the effective outlet to inlet gap ratio is less than one, $\eta < 1$, due to the effect of the kinetic energy carried over to the downstream cavity. The map shows a large unstable region on the HPS for $St > 1$ and a narrow unstable interval on the LPS, which is characteristic of a seal with $\eta < 1$, as it has been described before.

The second scenario is generated by decreasing the nominal gap on the first fin to reach a geometric gap ratio of $\eta_g = 4/3$. The ratio of the discharge coefficients is very close to one ($C_{d,2}/C_{d,1} \simeq 0.94$) but the effect of the kinetic energy carried over to the exit makes that the effective outlet to inlet gap ratio is $\eta \simeq 1$. Figure 14 (b) shows in fact that the CV model stability criterion

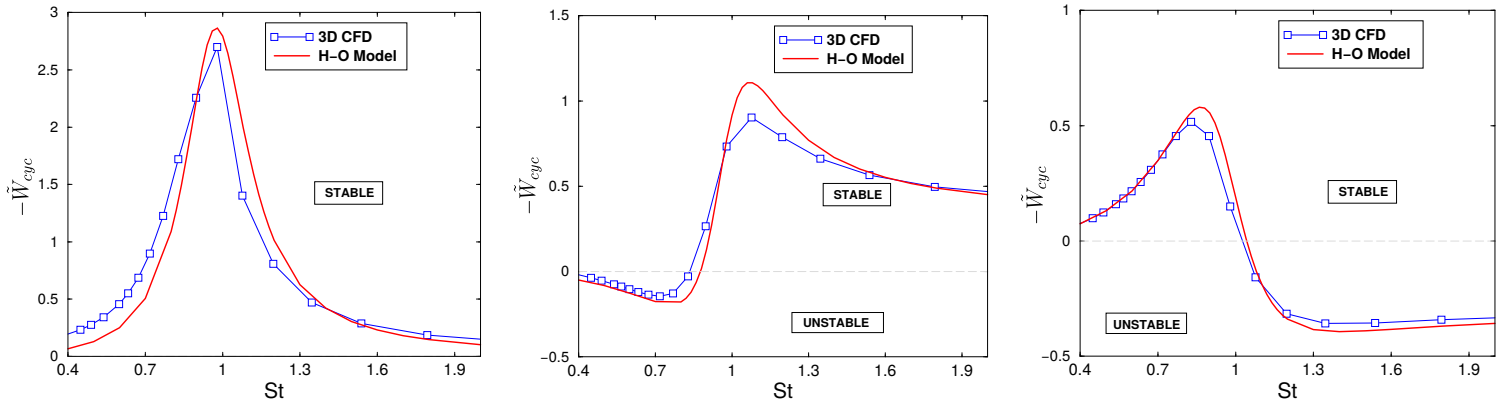

(a) $\eta_g = 1.$ $\tilde{e}h' = 1.5$ $(r/L = 15)$ (b) $\eta_g = 4/3.$ $\tilde{e}h' = 0.32$ $(r/L = 4)$ (c) $\eta_g = 2.$ $\tilde{e}h' = -0.05$ $(r/L = -0.5)$

FIGURE 15. NONDIMENSIONAL WORK-PER-CYCLE FOR A TWO-FIN STRAIGHT SEAL WITH DIFFERENT GEOMETRIC GAP RATIOS OPERATING AND TORSION CENTERS ($\pi_T = 1.5$). SOLID LINES: HIGH-ORDER CV MODEL [12]. SYMBOLS: LINEARIZED NAVIER-STOKES ANALYSES.

described in [9] is recovered. A seal supported on the LPS is unstable when $St \lesssim 1$, and unstable in a bounded region when the seal support is on the HPS. It is concluded that, to recover the CV stability criterion for nominally identical gaps, a differential gapping is required to ensure that $\eta \simeq 1$. The matching between the CV model and the simulations is excellent.

Finally, the case in which the outlet gap doubles the first, $\eta_g = 2$, is presented. This situation is not common, and usually never considered as the design intent. However, it is representative of a case in which due to rubbing and contact with the static parts, the second fin has been deteriorated or even worn out completely. This configuration is benign and robust since tends to stabilize seals supported on the HPS and to deteriorate slightly the stability of seals supported on the HPS, which are always stable if $St > 1$. There is always a narrow unstable region close to $\tilde{e}_{eff}h' = 0$ on the HPS. The degree of matching of the analytical model with the CFD predictions is surprisingly good.

Concerning seal deterioration, the worst-case scenario arises when the inlet seal is eroded or partially removed. In this case, stable seals supported either on the LPS or the HPS can become unstable unexpectedly. This can be seen in Fig. 12 (a) where the stability map for $\eta = 0.5$ obtained with the model is plotted. The high-frequency seal modes are always unstable except if the torsion center is located in the LPS close to $\tilde{e}_{eff}h' = 0$.

Figure 15 is intended to display a more quantitative comparison between the model and the simulations. This figure compares the $\tilde{W}_{cyc}$ obtained by the model and the linearized Navier-Stokes simulations for a constant torsion center and varying St, for the same seal and pressure ratio ($\pi_T = 1.5$). The vibration-to-acoustic ratio is changed varying the ND and keeping constant the frequency of vibration, exactly as it was done to obtain the stability maps. Different samples of Fig. 14 including cuts at the LPS and HPS have been selected. The actual physical and dimensionless position of the cuts are given in the caption of Fig. 15. It can be seen that the actual shape of the curves varies significantly from case to case but the level of matching between the model and the simulation is good in all the cases.

It is concluded that the CV model if properly fed with the correct parameters can reproduce the results obtained using linearized Navier-Stokes simulations.

CONCLUDING REMARKS

The baseline CV model for labyrinth seal flutter has been explored in detail to invetigate the impact the effect of dissimilar gaps. The different closure of the inlet and outlet gaps can be either geometric or induced by the flow. There are two mechanisms that give rise to the effective gaps. The first is the contraction of the streamlines at the gap inlet due to flow separation in the fin seal. This phenomenon is accounted for using the classical concept of discharge coefficient. The second has to do with the partial recovery of the kinetic energy of the incoming jet on the downstream closure. This effect is retained using the so-called carry over coefficient. Unlike the discharge coefficient, the kinetic energy carry-over coefficient entails a non-negligible modification of the underlying model that finally can be recast in the same for as the original one if the proper effective gaps are used in the non-dimensionalisation of the problem.

It is shown that seal stability is very sensitive to the gap ratio and that a seal supported on the LPS can behave as if it were physically supported on the HPS. The analytical analysis of the stability of the problem as a function of the dimensionless parameters is simple but the results are difficult to express simply. It was finally decided to focus on the operating conditions which are of interest for the industry including the main and clearest conclusions.

It is concluded that straight-through seals designed with nominal gaps are not robust against small perturbations of the gaps and in practice behave as seal with the first gap more open than in nominal conditions. For the typical range of the seal design parameters, perturbations of the design intent leading to values of the gap ratio slightly smaller than one ($\eta \lesssim 1$) make the seal can behave very differently than predicted by the baseline CV model. Small perturbations of the nominally equal seal gaps can lead to a more unstable seal than originally foreseen.

The motivation for modifying the formulation was the inability of matching the model with the simulations in some particular cases. A large simulation matrix of 3D frequency-domain linearized Navier-Stokes simulation has been included to support all the claims discussed in this work. The model and the simulations exhibit and excellent degree of matching in the whole range of parameters. It is concluded that the model can be used to make quantitative predictions as well.

ACKNOWLEDGMENTS

Roque Corral and Michele Greco want to thank ITP Aero by providing access to ITP's computing framework and its support. This research work has been partially supported by the European project ARIAS, H2020 research and innovation program under grant agreement No. 769346. The authors gratefully acknowledge the financial support.

NOMENCLATURE

$a_j(t)$	$j-th$ gap time perturbation
a_0	Sound speed in the cavity
A	Seal clearance area
C_d	$=\dot{m}/\dot{m}_{id}$., Discharge Coefficient
CV	Corral and Vega
h	Upstream fin non-dimensional pressure function
H	Fin clearance
HPS	High Pressure Side
L	Seal cavity length
LPS	Low Pressure Side
$\dot{m}$	Mass flow per span-wise or circumferential length unit
ND	Nodal diameter
p_c	Cavity static pressure
p_e	Exit static pressure
P_0	Inlet total pressure
r	Torsion center position
R	Cavity radius
Re	$=\dot{m}/(2\pi R\mu)$ Reynolds number based on the gap
R_g	Specific gas constant
s	Cavity height
$\bar{s}$	$=s/(\gamma H h')$, Nondimensional cavity height
J	Downstream fin non-dimensional pressure function
St	$=\frac{\omega R}{ND\,a_0}$. Vibration-to-acoustic frequency ratio
t	Tip fin thickness
t_d	$=\frac{p_{c,s}V_{c,s}}{\dot{m}_s a_0^2}$. Discharge time
TC	Torsion center
v_θ	Circumferential velocity
W_{cyc}	Work per cycle
z	Azimuthal coordinate

Greek symbols

β	Jet opening angle
χ	kinetic energy carry-over coefficient
γ	Heat capacity ratio
η	$=H_2/H_1$. Gap ratio.
π_s	$=P_0/p_c$. Cavity pressure ratio
π_T	$=P_0/p_e$. Total pressure ratio
π_c	$=\pi_T/\pi$. Pressure ratios relationship
ω	Vibration angular frequency (rad/s)
Ω	$=\omega t_d$ Non-dimensional discharge time
$\tilde{\Omega}$	$=\tilde{\Omega}/h'$. Ω rescaling with π_T
ρ	Fluid density
$\Delta\theta$	Rotation angle
τ	Non-dimensional time

Super-scripts

˜	Non-dimensional values
'	Time perturbation

Sub-scripts

e	Exit
f	Fluid dynamic
g	Geometric
0	Total property
c	Cavity
cyc	cycle
s	Steady state
eff	Effective value

References

[1] Chupp, R., Hendricks, R., Lattime, S., and Steinetz, B., 2006. "Sealing in turbomachinery". *AIAA Journal of Propulsion and Power,* **22**(2), March, pp. 314–349.

[2] Alford, J., 1964. "Protection of labyrinth seals from flexural vibration". *ASME J. Eng. Gas Turbines Power,* **86**(2), October, pp. 141–147.

[3] Alford, J. S., 1971. "Labyrinth seal designs have benefitted from development and service experience". In SAE Technical Paper, SAE International.

[4] Alford, J. S., 1975. "Nature, causes and prevention of

labyrinth air seal failures". *AIAA Journal of Aircraft,* **12**(4), April, pp. 313–318.

[5] Lewis, D., Platt, C., and Smith, E., 1979. "Aeroelastic instability in F100 labyrinth air seals". *AIAA Journal of Aircraft,* **16**(7), pp. 484–490.

[6] Ehrich, F., 1968. "Aeroelastic instability in labyrinth seals". *ASME J. Eng. Gas Turbines Power,* **90**(4), October, pp. 369–374.

[7] Abbot, D. R., 1981. "Advances in labyrinth seal aeroelastic instability prediction and prevention". *ASME J. Eng. Gas Turbines Power,* **103**(2), April, pp. 308–312.

[8] Mare, L. D., Imregun, M., Green, J., and Sayma, A. I., 2010. "A numerical study on labyrinth seal flutter". *ASME J Tribology,* **132**(2), pp. 022201–7.

[9] Corral, R., and Vega, A., 2018. "Conceptual flutter analysis of labyrinth seals using analytical models. part I: Theoretical background". *ASME J. Turbomach.,* **140**(10), October, p. 121006.

[10] Corral, R., Vega, A., and Greco, M., 2020. "Conceptual flutter analysis of stepped seals". *ASME J. Eng. Gas Turbines Power,* **142**(7), July, p. 071001.

[11] Corral, R., Greco, M., and Vega, A., 2019. "Tip-shroud labyrinth seal impact on the flutter stability of turbine rotor blades". *ASME J. of Turbomachinery,* **141**(10), October, p. 101006.

[12] Corral, R., Greco, M., and Vega, A., 2021. "Higher-order conceptual model for seal flutter". *ASME J. of Turbomachinery,* **143**(7), July, p. 071006.

[13] Greco, M., and Corral, R., 2021. "Numerical validation of an analytical seal flutter model". *Journal of the Global Power and Propulsion Society,* **5**, pp. 191–201.

[14] Miura, T., and Sakai, N., 2019. "Numerical and experimental studies of labyrinth seal aeroelastic instability". *ASME J. Eng. Gas Turbines Power,* **141**(11), November, p. 111005.

[15] Vega, A., and Corral, R., 2018. "Conceptual flutter analysis of labyrinth seals using analytical models. Part II: Physical interpretation". *ASME J. Turbomach.,* **140**(10), October, p. 121007.

[16] Hodkinson, B., 1939. "Estimation of the leakage through a labyrinth gland". *Proceedings of the Institution of Mechanical Engineers,* **141**, pp. 283–288.

[17] Burgos, M., Corral, R., and Contreras, J., 2011. "Efficient edge based rotor/stator interaction method". *AIAA Journal,* **41**(1), January, pp. 19–31.

[18] Suryanarayanan, S., and Morrison, G. L., 2009. "Analysis of flow parameters influencing carry-over coefficient of labyrinth seals". In ASME Paper GT2009-59245, Vol. 3 of *ASME Turbo Expo 2009*, pp. 1137–1145.

[19] Szymanski, A., Dykas, S., Majkut, M., and Strozik, M., 2016. "The assessment of the calculation method for determining characteristics of one straight fin labyrinth seal". *Transactions of the Institute of Fluid-Flow Machinery,* **134**, pp. 89–107.

[20] Corral, R., Escribano, A., Gisbert, F., Serrano, A., and Vasco, C., 2003. "Validation of a linear multigrid accelerated unstructured navier-stokes solver for the computation of turbine blades on hybrid grids". In AIAA Paper 2003-3326, 9th AIAA/CEAS Aeroacoustics Conference.

[21] Vega, A., and Corral, R., 2016. "The low reduced frequency limit of vibrating airfoils - Part II: Numerical experiments". *ASME J. Turbomach,* **128**(2), February, p. 021005.

[22] Corral, R., Beloki, J., Calza, P., and Elliot, R., 2019. "Flutter generation and control using mistuning in a turbine rotating rig". *AIAA Journal,* **57**(2), February, pp. 782–795.